

Activity-based contact network scaling and epidemic propagation in metropolitan areas

Nishant Kumar¹, Jimi B. Oke², and Bat-hen Nahmias-Biran³

¹ETH Zurich, Future Resilient Systems, Singapore-ETH Centre, Singapore 138602

²Department of Civil and Environmental Engineering, University of Massachusetts, Amherst, MA 01003, United States

³Department of Civil Engineering, Ariel University, Ariel 40700, Israel

August 3, 2020

Abstract

Given the growth of urbanization and emerging pandemic threats, more sophisticated models are required to understand disease propagation and investigate the impacts of intervention strategies across various city types. We introduce a fully mechanistic, activity-based and highly spatio-temporally resolved epidemiological model which leverages on person-trajectories obtained from integrated mobility demand and supply models in full-scale cities. Simulating COVID-19 evolution in two full-scale cities with representative synthetic populations and mobility patterns, we analyze activity-based contact networks. We observe that transit contacts are scale-free in both cities, work contacts are Weibull distributed, and shopping or leisure contacts are exponentially distributed. We also investigate the impact of the transit network, finding that its removal dampens disease propagation, while work is also critical to post-peak disease spreading. Our framework, validated against existing case and mortality data, demonstrates the potential for tracking and tracing, along with detailed socio-demographic and mobility analyses of epidemic control strategies.

Introduction

As the COVID-19 pandemic caused by the SARS-CoV-2 virus continues to ravage populations worldwide, there is a dire need to better understand the propagation of epidemics in order to mitigate its inimical effects in various communities. Cities, in particular, have been hit hard due to their population density and extensive mass transit systems [1]. Governments across the world have responded by imposing varying levels of mobility restrictions and social distancing [2]. Large amounts of data have been generated to track the spread of the disease (infection, recovery and death rates). Given the mixed results from these interventions, more sophisticated tools are required to enable decisionmakers to accurately predict the trajectory of the disease, as well as model the unknown effects of mitigating strategies. Hence, agent-based simulations (ABMs) are critical to this effort. With modern computational advances, ABMs have demonstrated great potential in accurately tracking the spread of an epidemic at multiple levels [3]. Many of the prior agent-based models were low-resolution and relied on broad approximations regarding the trajectories of the populations being represented [3]. Recent high-resolution efforts, however, have taken advantage of detailed cellphone data, as well as microscopic traffic simulations [4]. With a granular representation of agent movements, more realistic epidemic simulations can be conducted. Modeling epidemic spreading using an agent-based approach pursues the progression of a disease through each individual, and tracks the contacts of each individual with others in the relevant social and geographical networks [5].

Agent-based models capture the complexity of human mobility and social patterns more richly than the classical approaches [2, 3]. Mesoscopic and microscopic transportation models provide an even more detailed representation of the activity behavior and physical network [6]. Only recently have these models been utilized in the study of disease propagation [3]. While the transportation-based model in [3] reasonably approximated the observed event (seasonal influenza in 2016/2017), socio-demographic factors were not considered with regard to susceptibility. Likewise, the agent interactions during public transport usage were not considered and only a small scale demonstration was performed (1% of the actual population of Zurich). Most recently, [4] created a contact network from the trajectories obtained from cellphone data to study the impact of various epidemic mitigation scenarios related to COVID-19. However, they could not perform detailed contact tracing, and only a sample of the population was used. Notably, a recent effort modeled the spatial patterns of the Switzerland 2003/04 influenza epidemic [7]. Susceptibility varied according to two age groups but contact duration and intensity were not included in the model. Thus, the time-resolution was only at the day level and estimates were made regarding contacts by activity (using only a subset of the potential contacts encountered by each individual). The spread of COVID-19 in Wuhan, China, has also been simulated using an age and location-specific model [8]. However, this effort did not account for the effects of transit and actual person movements.

In this study, we close the gap identified in previous efforts. We layer a mechanistic agent-based epidemiological model (PanCitySim) onto highly time-resolved and spatially disaggregated daily person-trajectories obtained from a microscopic travel demand and mesoscopic supply simulator, SimMobility [6] (see Figure 1). This framework provides a realistic representation of person and vehicle movements in an average day for a full-scale city [9]. We generate activity-specific five-minute contact graphs for the entire population and explore their scaling properties. We demonstrate how PanCitySim can be used to not only predict the spatio-temporal dynamics of an epidemic, but also provide detailed contact-tracing and individual-level analyses of disease impacts. The epidemiological framework is fully stochastic, taking into account the latest measurements of relevant parameters, such as the incubation period, duration of infectiousness, and age-dependent likelihood of symptomaticity and mortality [4, 8, 10, 11]. Thus, we exploit the rich activity simulation

Results

A recent study identified 12 urban typologies based on 69 mobility, socio-demographic, environmental and network structure obtained from over 300 cities [9]. The two auto-dependent typologies consisting of cities largely in the US/Canada were used as the test beds for this study: *Auto Sprawl* (86% car mode share) and *Auto Innovative* (78% car mode share). *Auto Sprawl* (e.g. Baltimore, Tampa, Raleigh) typifies the lower-density US/Canada cities with low transit usage ($\sim 4\%$), while *Auto Innovative* (e.g. Washington D.C., Atlanta, Boston) are denser cities with an average of 11% transit mode share. Prototype cities representing the population, land-use and mobility demand and supply outcomes in both typologies were synthesized (see Methods and [13]). Both prototype cities are built on actual road and transit networks, population microdata and land use categories from representative (or archetype) cities close to the centroid of their respective typologies. For *Auto Sprawl*, the archetype chosen is the Baltimore Metropolitan Area (population 2.77×10^6 , density $4.11 \times 10^2 \text{km}^{-2}$), while for *Auto Innovative*, it is Greater Boston (population 4.6×10^6 , density $5.09 \times 10^2 \text{km}^{-2}$). However, the demand and supply models for both prototype cities were calibrated to fit average typology values, in order to ensure representativeness of overall mobility outcomes. The spatio-temporal activity and mobility patterns of each city are shown in Figure 2.

Analysis of contact network structure

We generate an activity-based contact network for the population in each city every 5 minutes (see Methods). The *Union* contact network comprises all activities for each individual: *Work*, *Education*, *Shopping*, *Other* and *Transit*. In this paper, the *Transit* activity comprises waiting and the duration of time spent on a bus or train. The spatial resolution of each contact is at the node level (activity location) or in transit vehicle (bus/train) partitions. Figure 3a shows the degree distribution for the *Union* contact network at selected times in both cities. Further, we plot the average degree $\langle k \rangle$ for each activity contact network, including the *Union*. We observe that *Work* is responsible for the maximum average number of contacts, peaking at 10 AM with 90 contacts in *Auto Sprawl* and 120 in *Auto Innovative*. In *Auto Sprawl*, the activity responsible for the second highest average number of contacts per time step is *Transit* with 70 contacts on average at morning peak (8 AM) and almost 80 contacts on average at evening peak (3 PM). In *Auto Innovative*, however, the activity responsible for second greatest peak contact average is *Shopping* with 110 contacts per person between 4 and 5 PM.

We also plot the average weighted degree distribution $\langle k_w \rangle$ (Figure 3c), weighting each edge by $\frac{1}{d_{nm}}$, where d_{nm} is the estimated distance between persons n and m at a given node at a time step. The distribution of $\langle k_w \rangle$ reveals that *Transit* is responsible for the closest contacts, and that *Shopping* is less important than *Work* in terms of proximity. The difference between the average separation of contacts in *Auto Sprawl* is close to two orders of magnitude. The disparity is less stark (less than one order of magnitude) in *Auto Innovative*, given its greater population density). The maximum number of people who are in contact at any given time of the day is represented by the maximum clique size of the contact graph as shown in Figure 3d. On average, the maximum number of contacts created in *Auto Sprawl* is more than 1600 between 10 and 11 AM, while for *Auto Innovative* the maximum number of contacts is twice as high during the same time.

Scaling properties of time-dependent contact graphs

In order to gain further insights into the contact network structure, we plot the complementary cumulative distribution functions (CCDF) for each time step (5 minutes) in both cities (Figure 4).

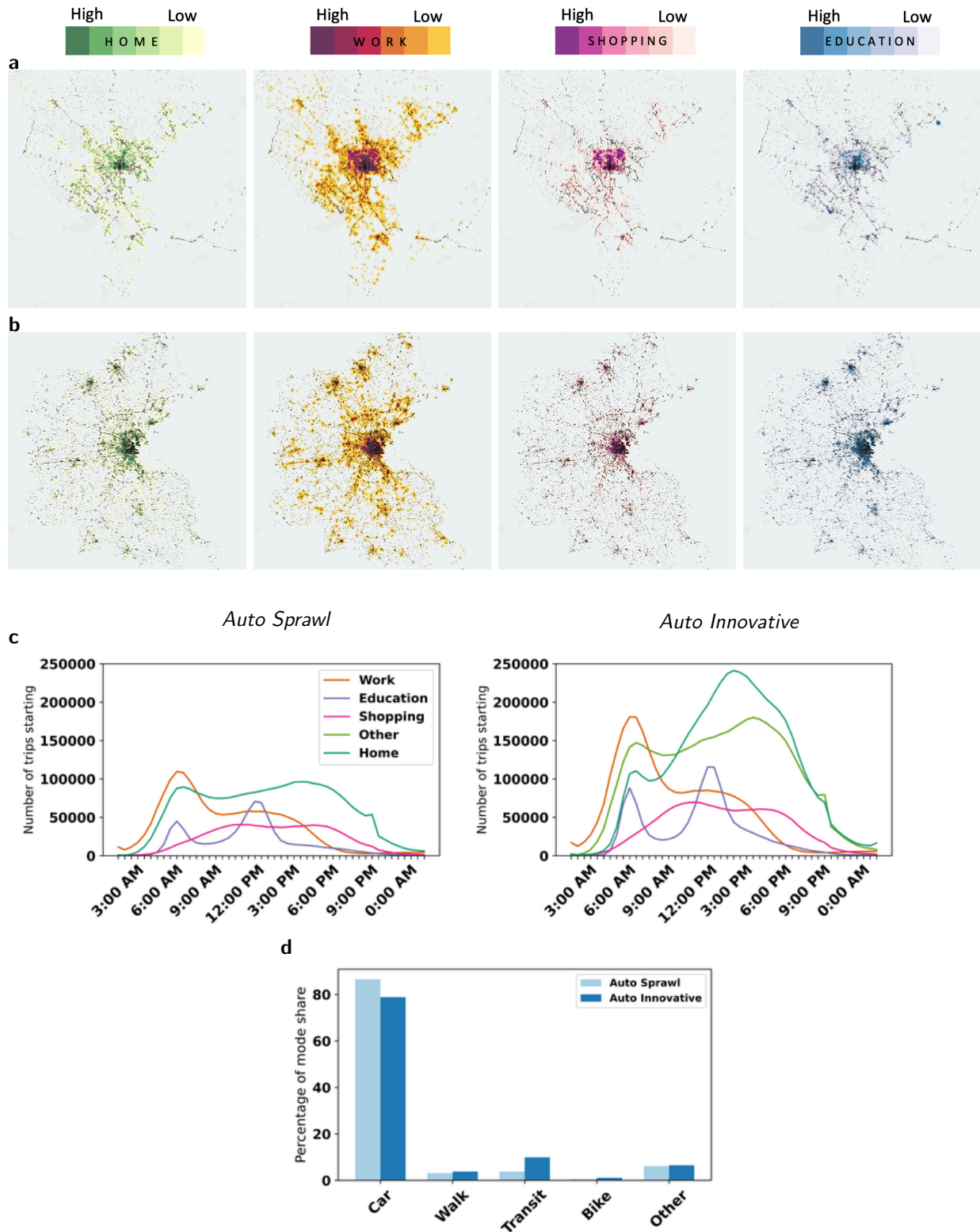


Figure 2. Activity and mobility patterns in prototype cities. Spatial distribution of activity locations in **a** *Auto Sprawl*, and **b** *Auto Innovative*. The radii of heat maps are the same across both the cities; **c** Number of trips starting at various 30-minute intervals during the day; **d** Mode share for the two cities. Daily number of trips in *Auto Sprawl* is 9.72×10^6 , while in *Auto Innovative* it is 16×10^6 . Both cities have a similar trip generation rate of 3.5 per person.

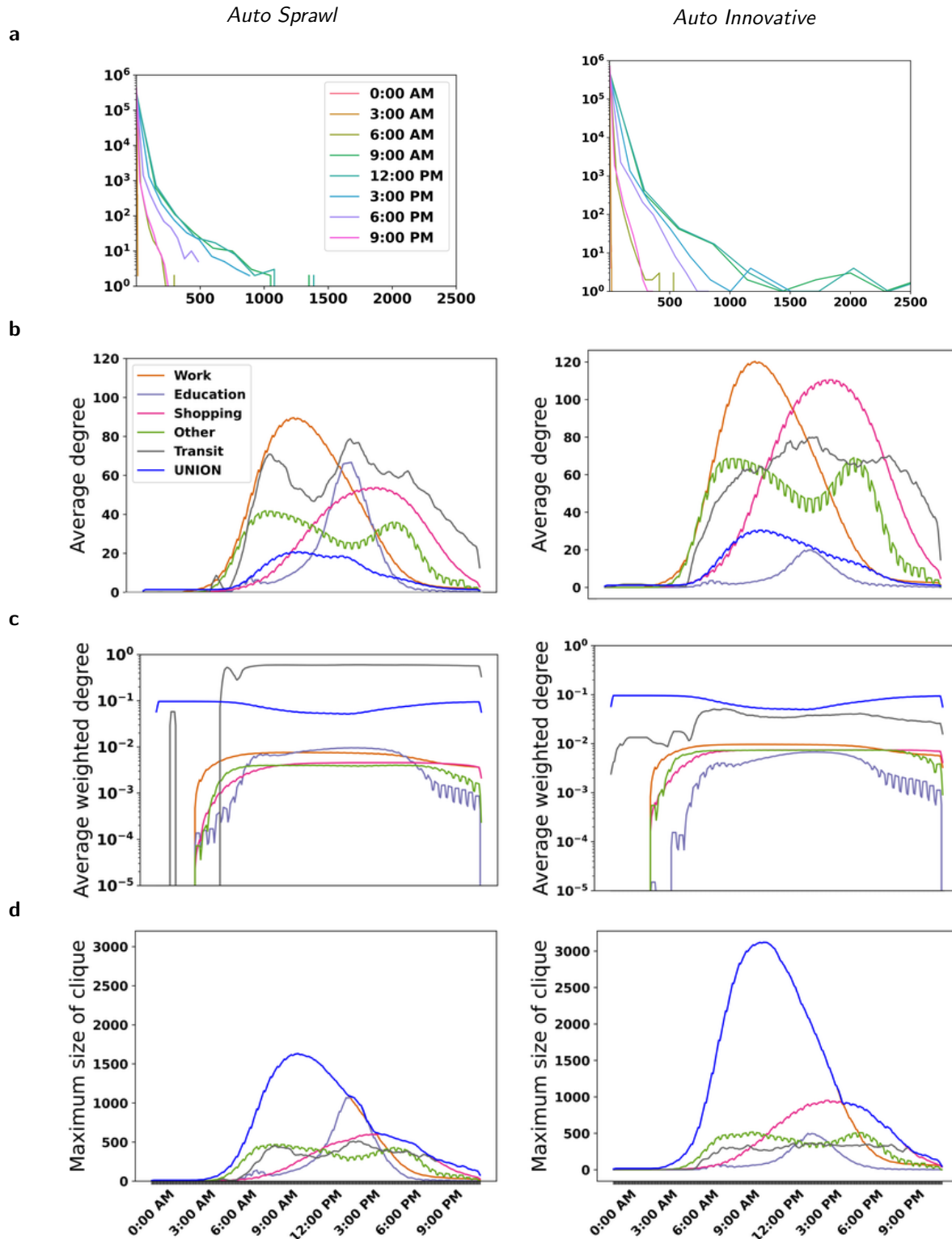


Figure 3. Contact network structure. **a** Degree distributions of the *Union* contact network for selected times of day; **b** The average degree $\langle k \rangle$ for both cities are shown over the course of the day; **c** The average weighted degree $\langle k_w \rangle$ for both cities are shown over the course of the day using log scale). Contacts are weighted by average inverse distances between persons at each node; **d** Diameter (maximum clique size). We see that *Work* accounts for the greatest number of contacts per person, particularly during the middle of the day. However, the distribution of $\langle k_w \rangle$ indicates that *Transit*, more than any other activity, accounts for the closest of contacts. For clarity, plots are smoothed using a moving average of five time steps.

The CCDFs are shown for the *Union* contact graphs, as well as for each of the activities including *Transit*. There are no clear patterns in the union contact graphs, but we hypothesize that the *Work* contact network follows a Weibull distribution $p_k \propto e^{(-\lambda k)^\beta}$, while the *Transit* contact network obeys the power law, $p(k) \propto k^{-\alpha}$. Contact networks for *Shopping* and *Other* activities appear to follow an exponential distribution $p_k \propto e^{-\lambda k}$. In order to test these null hypotheses, we conduct Kolmogorov-Smirnov (KS) tests to determine if alternative distributions provide better fits [14]. The KS tests produce p-values based on loglikelihood ratios between the alternative and null fits. In all cases, there was no sufficient evidence to reject the null hypothesis. The fitted distributions are assumed to be valid from a minimum degree \hat{k}_{\min} , which is determined by minimizing the KS-distance between observed and predicted values based on the power law fit. While this \hat{k}_{\min} is biased, it facilitates a consistent comparison between candidate distributions [15]. Other alternative distributions considered were the lognormal and truncated power law.

The scale-free *Transit* contact graphs are fitted to $p_k \propto k^{-\hat{\alpha}}$, with a cut-off at $k = 150$. Between 8 AM and 8 PM, $\hat{\alpha} \approx 1.4$ in both cities. The parameter \hat{k}_{\min} is largely time-invariant, averaging 2.4 in *Auto Sprawl* and 2.2 in *Auto Innovative* (Figure 5d). This indicates that fitted scaling patterns take effect with a minimum of two or three contacts. For *Shopping*, which follows an exponential distribution, $\hat{\lambda}$ is similar for both cities at the same time periods. In the case of *Other*, however, while the trends in *Auto Sprawl* and *Auto Innovative* are similar, $\hat{\lambda}$ tends to be higher in *Auto Sprawl*. The fitted Weibull parameters for *Work* diverge between both cities (Figure 5c).

Spatio-temporal evolution and age-specific impacts

We calibrated *Auto Sprawl* and *Auto Innovative* to fit the expected early dynamics of COVID-19 [8, 16, 17, 18] (see Methods). We considered the basic reproductive rate R_0 (average number of secondary infections per index case), which ranged from 2.29 to 2.57 in *Auto Sprawl*, and from 3.03 to 3.35 in *Auto Innovative*. Given the uncertainty about R_0 , we also considered the time-dependent reproduction number R_t (average number of new daily infections per infectious individuals). We compute the five-day average of R_t as a measure of the early propagation of the epidemic, which is 0.77 in both cities (see Methods). Given these starting assumptions, we simulate the epidemic for 270 days in both cities. The peak number of infections occurs at day 27 in *Auto Sprawl* and at day 34 in *Auto Innovative*, dissipating after 150 days and 250 days, respectively. At the peak, there are 9.21×10^4 infections (both exposed and infectious individuals) in *Auto Sprawl* and 1.27×10^5 infections in *Auto Innovative* (Figure 6b).

We plot the daily infection and mortality rates, along with R_t in Figure 6c. The infection rate is given by the number of daily new infections as a proportion of the entire population. The mortality rate is defined as the number of daily deaths also with respect to the entire population. While both *Auto Sprawl* and *Auto Innovative* have similar early onset dynamics, we observe that disease propagation diverges rapidly between both cities. In *Auto Sprawl*, R_t peaks at day 9, with an average rate of change of $1.78 \times 10^{-1} \text{ day}^{-2}$ from onset to peak. Post-peak, however, the rate of change is $-9.61 \times 10^{-3} \text{ day}^{-2}$. Furthermore, the slope of the infection rate from onset to peak (day 18) in *Auto Sprawl* is $5.15 \times 10^2 \text{ day}^{-2}$. Post-peak, the rate is $4.25 \times 10^1 \text{ day}^{-2}$. In *Auto Innovative*, however, R_t peaks at day 13, with a slope of $1.99 \times 10^{-1} \text{ day}^{-2}$ from onset. R_t then dissipates more slowly at a rate of $-3.94 \times 10^{-3} \text{ day}^{-2}$. The infection rate peaks at day 26 in *Auto Innovative* (twice the amount of time as in *Auto Sprawl*) at a rate of $4.52 \times 10^2 \text{ day}^{-2}$, and dissipates at a rate of $-5.44 \times 10^1 \text{ day}^{-2}$. From onset to peak, the mortality rate is similar in both cities: 1.34 day^{-2} in *Auto Sprawl* (peak: day 28) and 1.34 day^{-2} in *Auto Innovative* (peak: day 34).

Given that we used age-specific probabilities (for symptomaticity and mortality) in our SEIRD model, we can also observe the evolution of COVID-19 by age group in Figure 7a-d. Susceptibilities

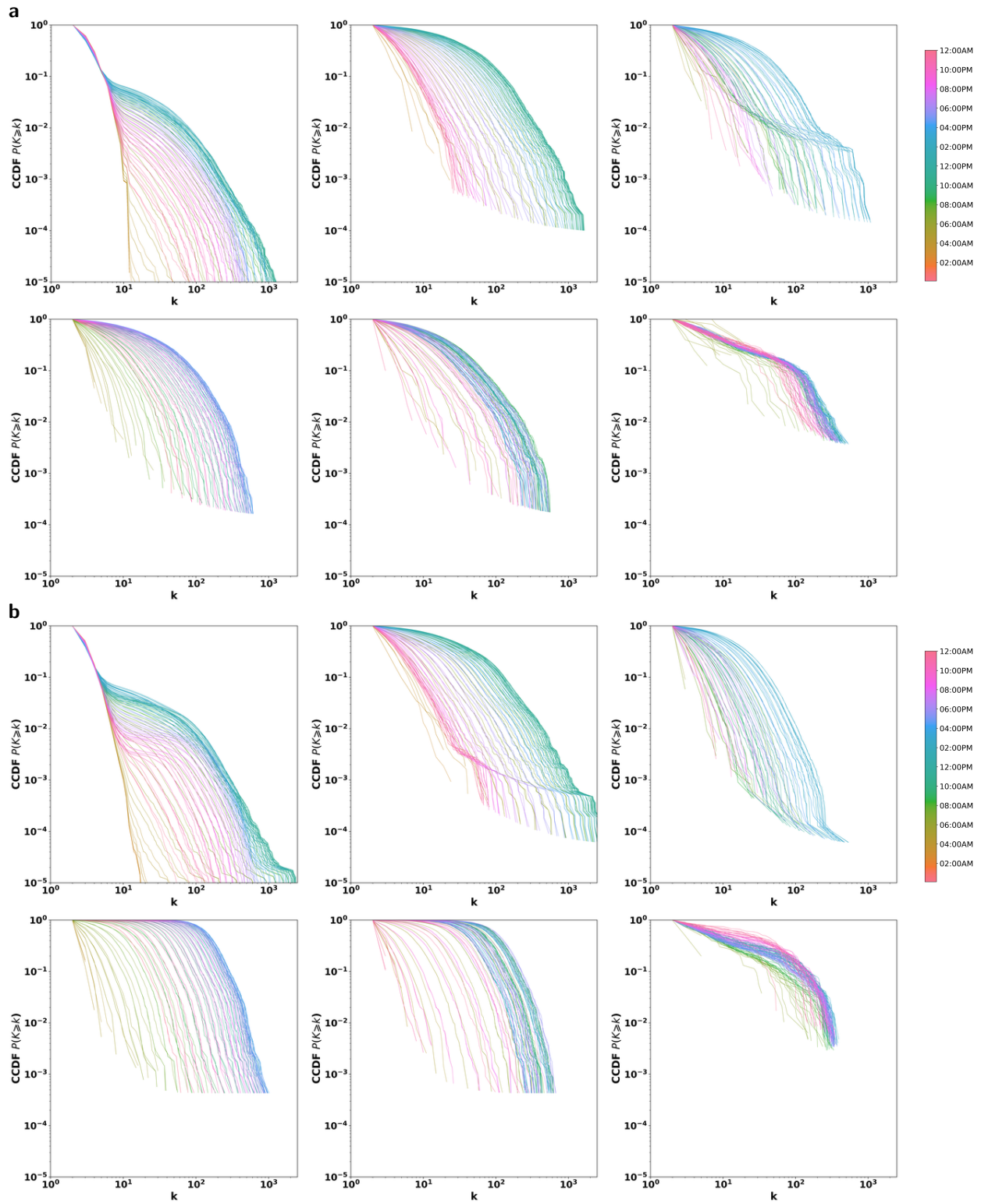


Figure 4. Activity-based contact networks. Complementary cumulative distribution (CCDF) plots of time-dependent contacts (clockwise): *Union, Work, Education, Transit, Other* and *Shopping*: **a** *Auto Sprawl*; **b** *Auto Innovative*.

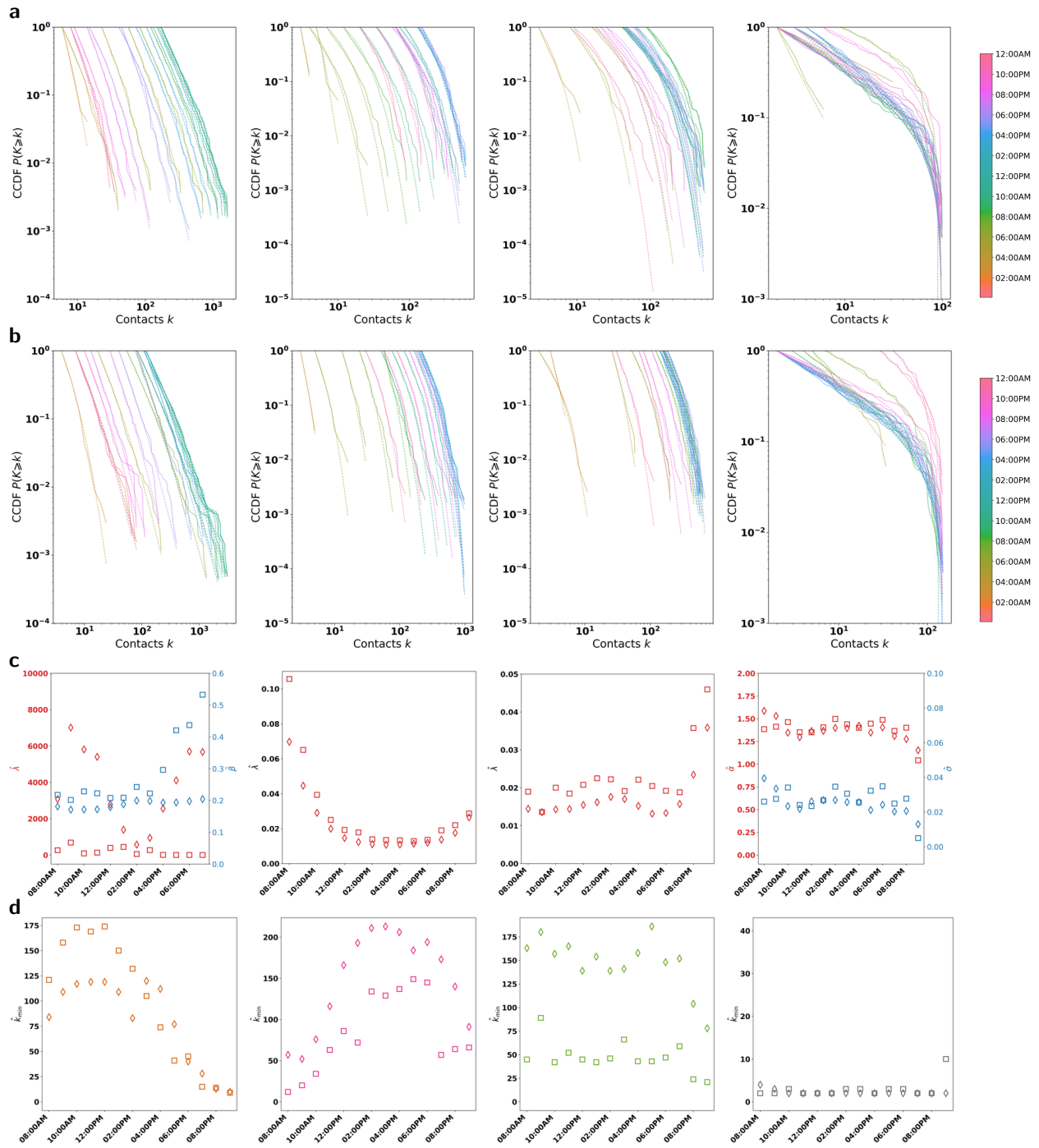


Figure 5. Contact network scaling. Fitted contact network degree distributions (dashed lines) compared to observed distributions from simulation (solid lines) shown for the respective activities: *Work*, *Shopping*, *Other* and *Transit*. Only hourly fits are displayed for clarity. **a** *Auto Sprawl*; **b** *Auto Innovative*. **c** Fitted parameters for *Auto Sprawl* (square markers \square) and *Auto Innovative* (diamond markers \diamond). *Work* follows a *Weibull* distribution, while *Shopping* and *Other* are fitted to exponential distributions. *Transit* is fitted to a power law. Parameters are only significant within time periods shown. **d** Fitted k_{\min} for each activity (*Work*, *Shopping*, *Other* and *Transit*). Time-dependence is exhibited for all activities except *Transit*.

are distributed as expected, with the oldest age category facing the highest fatalities. We also consider the evolution of the epidemic by activity (Figure 7e-f). At the onset of the epidemic, *Transit* activity is responsible for most of the transmissions, more so trains than buses. At peak infection, *Transit* remains responsible for the greatest share of transmissions in *Auto Sprawl*, while *Home* and *Work* have the greatest share in *Auto Innovative* (Figure 7f). In the latter stages, we find that the greatest share of infections occurs during *Work*. *Education* is also significant in *Auto Innovative* and *Shopping* in *Auto Sprawl*. The lowest impact activity is *Bus* transit.

We observe the spatial evolution of the epidemic in both cities (Figure 8). In *Auto Sprawl*, at the onset of the epidemic, we identify several hubs, mostly located outside of the city center. These quickly migrate to the city center by the second week, becoming stronger there, with the peak of the disease being observed in the sixth week. In *Auto Innovative*, a denser city with greater transit usage, the onset of the epidemic begins in city center, grows rapidly and spreads out to the suburbs. The peak of epidemic observed between weeks 5 and 7, after which there is a gradual decline of in the numbers throughout the city. We observe that towards the end of the simulation, the rate of decline is the number of cases is much slower for *Auto Innovative* compared to *Auto Sprawl*. At the end of our simulation period, *Auto Innovative* had around 10 times more active cases compared to *Auto Sprawl*.

Impact of transit network on disease propagation

To test the effect of the physical transit network on the propagation of the epidemic, we remove the *Transit* activity from the contact network construction in both *Auto Sprawl* and *Auto Innovative*. Then, we simulate the same COVID-19 dynamics on these no-transit models. We compare the SEIRD model outputs and time-dependent reproductive rates (Figure 6c). Results indicate that R_t peaks on the first day in *Auto Sprawl* (average value in the first five days is 1.40), dissipating at the rate of $-7.65 \times 10^{-3} \text{ day}^{-2}$. The removal of transit thus effectively dampens the reproduction of the epidemic from the onset in *Auto Sprawl*. In *Auto Innovative*, R_t peaks at day 25 (compared to day 13 in the full case), but its slope is now $4.29 \times 10^{-2} \text{ day}^{-2}$, five times smaller than in the full network. Thus, the force of the epidemic is also lessened in *Auto Innovative* by transit removal.

This effect is even more apparent when we consider the infection rates. In *Auto Sprawl*, the infection rate peaks at day 86 with 1.49×10^3 per day (compared to day 18 in the full network case, with 9.93×10^4 infections/day). Its slope (onset to peak) is $1.16 \times 10^1 \text{ day}^{-2}$ (44 times smaller than in the full case). Meanwhile, in *Auto Innovative*, the infection rate peaks at day 61 with 4.54×10^3 per day (compared to day 18 in the full network cases with 1.25×10^4 infections/day). It changes at a rate of $7.12 \times 10^1 \text{ day}^{-2}$ (6.4 times smaller than in the full case).

The force of mortality is also slowed, as daily deaths peak on day 62 in *Auto Sprawl* (compared to day 28 in the full case) and on day 78 in *Auto Innovative* (compared to day 34 in the full case). These results illustrate the importance of modeling the *Transit* contact network in detail, and the central role that public transportation plays in spreading the virus.

Discussion

In order to establish future epidemic protection programs in large metropolitan areas, it is necessary to analyze the effectiveness of multiple interventions and epidemic control policies on a large urban scale as well as among different communities and groups. For that purpose, we developed a flexible and dynamic framework, PanCitySim, which is built on a modified SEIRD model combined with an activity-based mechanistic model, which represents the urban environment and simulates

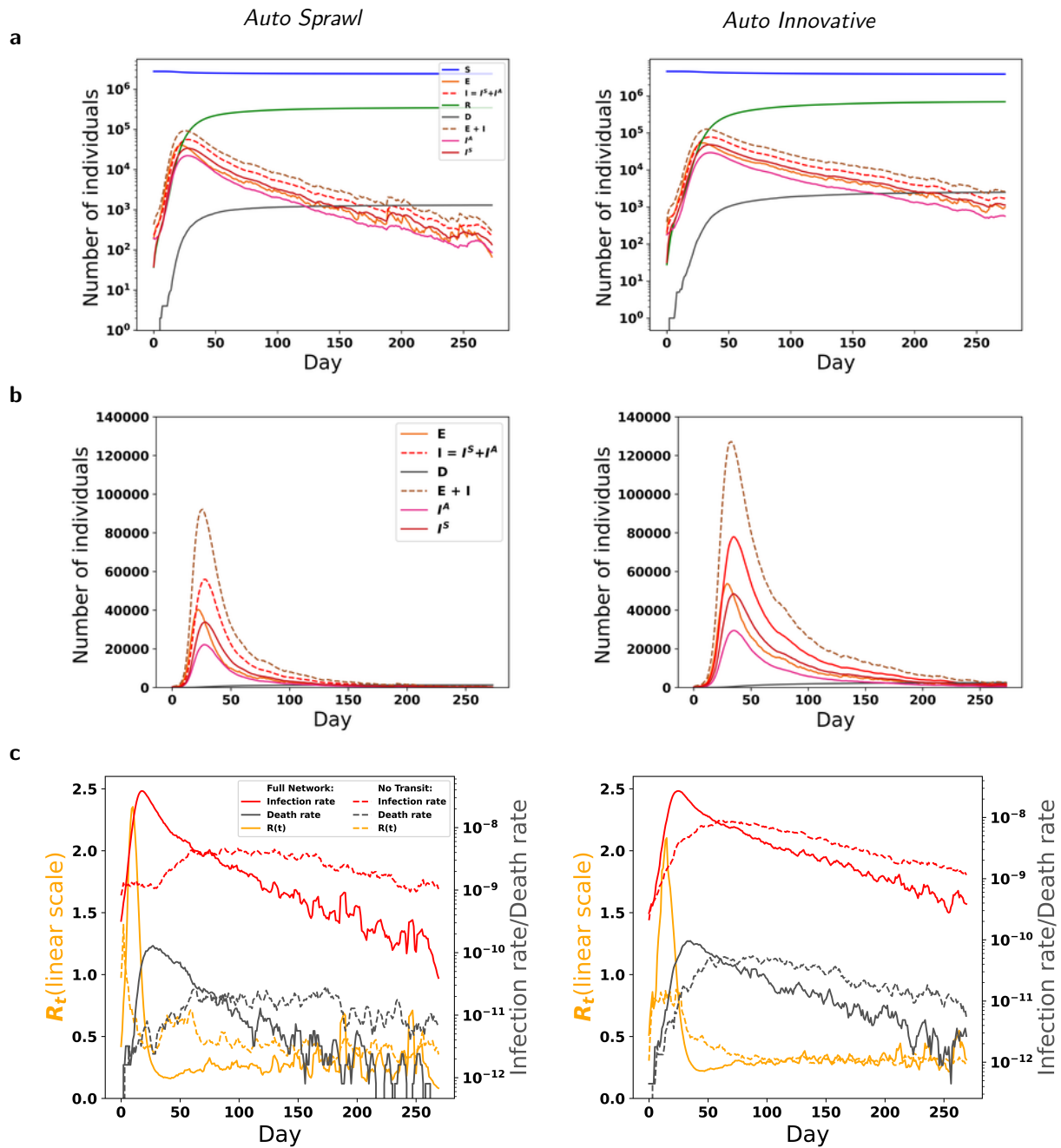


Figure 6. Simulated evolution of COVID-19 across two prototype cities. a Log y-axis of population states. **b** Exposed, infected (both asymptomatic and symptomatic cases) and deceased (cumulative). **c** Time-dependent (daily) reproductive rate R_t , infection and mortality rates. The curves are smoothed with a moving average over 5 days. The infection rate and death rate are expressed per 100,000 persons.

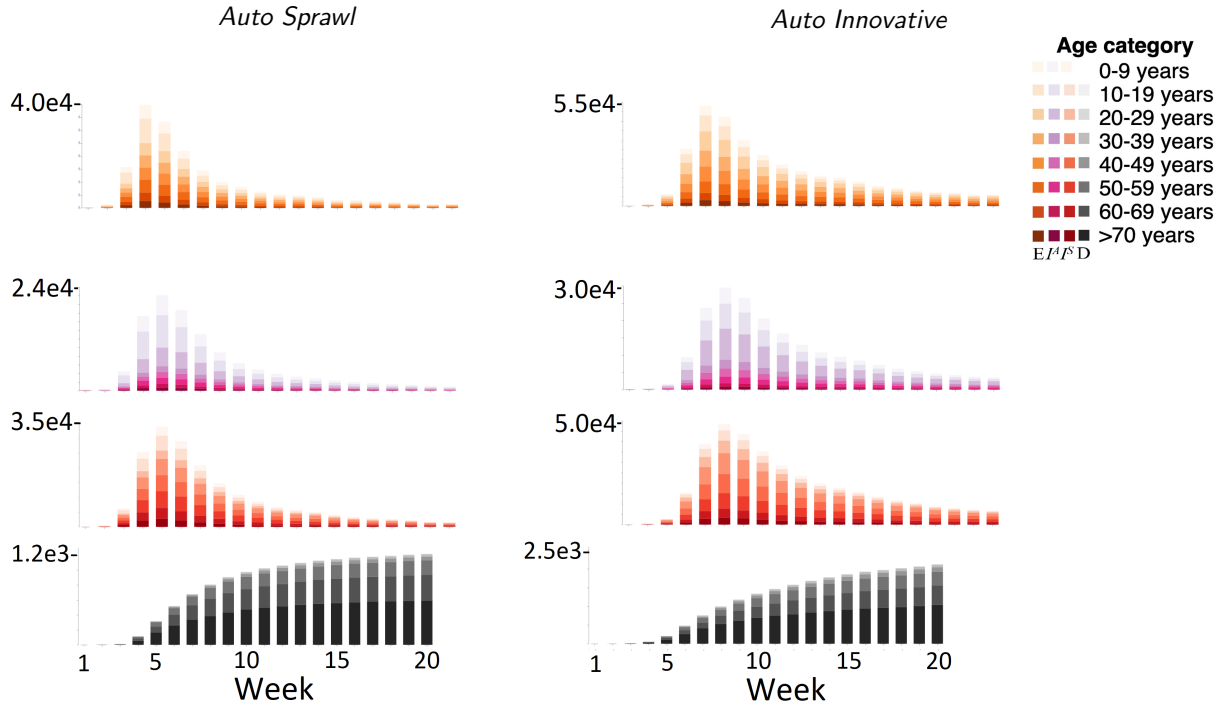


Figure 7. Propagation of COVID-19 by age.

population mobility and human interactions. We then introduced a modified SEIRD model incorporating the latest understanding of the propagation of COVID-19. The epidemiological model enables a computation of infection dynamics of the entire population in the city during their activities (including transit) at a 5-minute resolution. We demonstrate the use of PanCitySim and the rich output it provides in two prototype cities representative of most urban areas in the US and Canada (both auto dependent, but one with higher population density and greater share of mass transit).

Crucially, we generate 5-minute activity-based contact networks for entire synthetic populations. We found the largest average contacts per individual is 90 (in *Auto Sprawl*) and 120 (in *Auto Innovative*). We analyze the degree distributions of these networks, gaining important insights into the mixing of populations across two prototype cities representative of the US and Canada. Furthermore, we find that the activity contact networks follow well-known distributions describing complex systems. Contact networks for four activity types were fitted. Significantly, *Transit* contacts obey the power law ($\hat{\alpha} \sim 1.4$ up to a maximum of 150 contacts), which is time-invariant and constant in two distinct city types. *Shopping* and *Other* follow exponential distributions that are also largely time-invariant. *Work*, on the other hand, follows a Weibull (stretched exponential) distribution with time-dependent parameters differing by city. While *Work* accounts for the greatest number of contacts per person, particularly during the middle of the day, *Transit*, more than any other activity, accounts for the closest of contacts.

The inclusion of demographic variables, such as gender and age, introduces levels of susceptibility in different groups of individuals which is critical for a better understanding of disease propagation. We observed the dynamics of COVID-19 for 270 days in both cities, and found that even if the index cases begin on the outskirts of the city, the epidemic rapidly spreads to the city center. In both cities the epidemic peaks between days 27 and 34 with more than 9×10^4 infections, dissipating slowly after 150 days if the city is sparse or after 250 days for a denser typology with

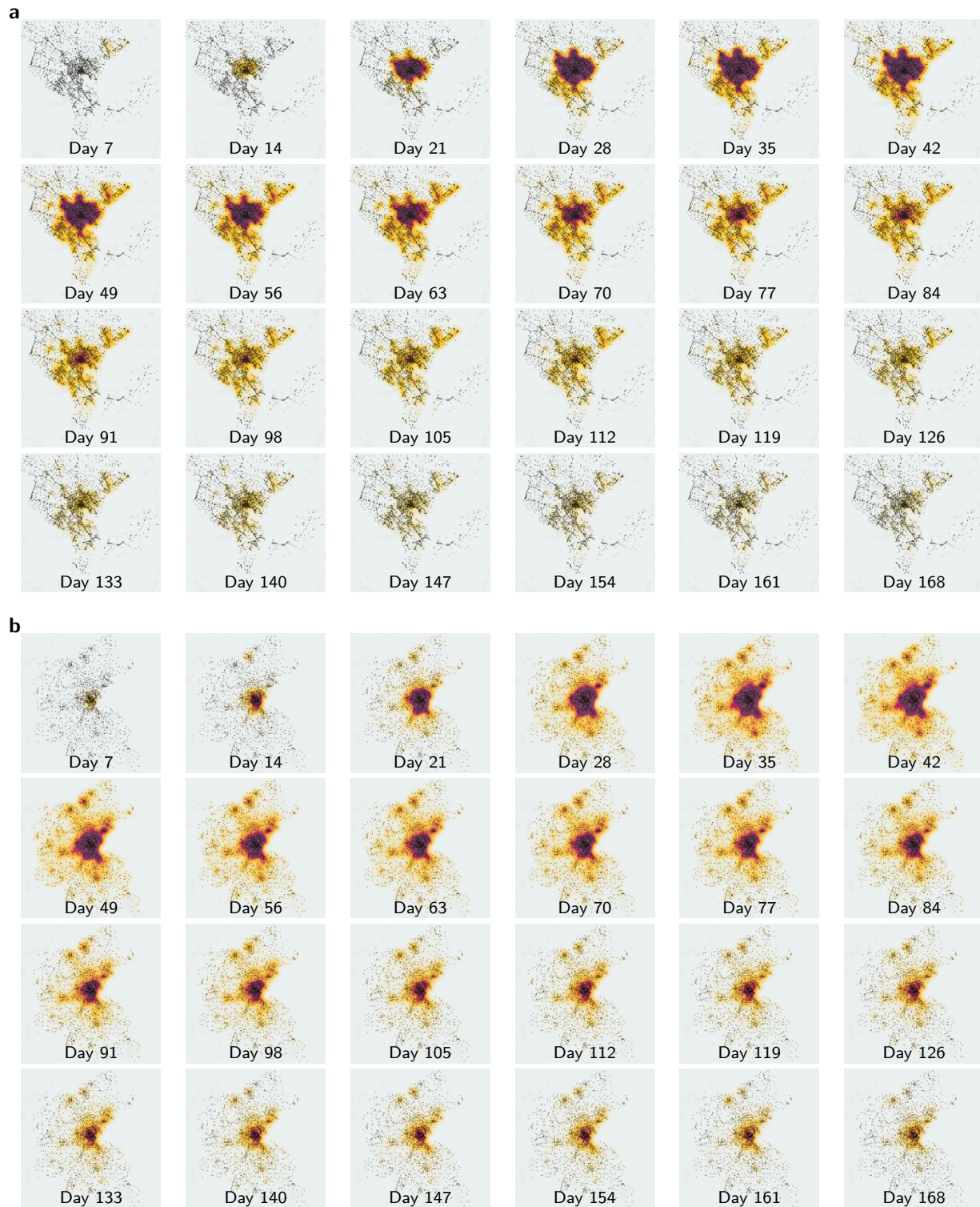


Figure 8. Spatial evolution of COVID-19. Heatmap of infected (exposed and infectious) individuals every seven days: **a** *Auto Sprawl*; **b** *Auto Innovative*. As expected, the prevalence is greatest in city centers, regardless of the location of index cases. In *Auto Innovative*, the hubs are evident.

more than 1.3×10^5 exposed or infected individuals.

Further, we found that at the onset of the epidemic it is crucial to restrict mass transit services or focus interventions (such as enforcing mask-wearing by passengers) on this activity. Post-peak, however, restrictions should be targeted towards work areas, as well as shopping centers or schools in less dense car-oriented cities. Our approach, which is fully mechanistic and highly spatio-temporally resolved, offers insights into the contact network structure and the importance of having a detailed representation of population mobility. With PanCitySim, scenarios can be realistically modeled and targeted to specific activities, ages, and employment types. We can detect the emergence of super-spreading events and show how urban activity patterns affects the spreading of such events. Further, there is a need to investigate the effects of network topology and reproduction rates R_0 and R_t . Future work also needs to be done to understand how index case locations affects disease propagation in urban areas.

Methods

Activity-based simulation model and city data

The simulation of the prototype cities is performed in SimMobility, an open-source platform for microscopic demand and mesoscopic supply dynamic traffic assignment modeling [6]. It is calibrated for modeshares, activity patterns and speeds in the cities we discuss. The calibration and validation details are available in [13]. The activity- and agent-based simulator takes as inputs: land use, demographic and economic factors, as well as road and transit networks. A discrete choice modeling framework then simulates daily activity schedules (DAS) for each individual in a given synthetic population. Parameters for population (including age, gender, employment, vehicle ownership and household characteristics), land use and road/transit networks are obtained from a real-world archetype city in the typology. The DAS is a high level plan, including only important choices, which are translated into trip chains. Lower level choices are made during the day when those plans are executed. During the day, agents are either performing an activity (*Home, Work, Education, Shopping* or *Other*) or executing a trip. During an activity, agents are stationary at one location and then, at the beginning of each trip, agents further detail their plan. Once the detailed plan is made and the start time is reached, the supply simulator moves the agent accordingly. Given the path of each traveler, the supply simulator produces the actual movement trajectory of each heterogeneous vehicle type and pedestrian (passenger) movements, which are performed on the network to provide event-driven trajectories for each person.

From the 5-minute person-trajectories, activity-specific contact graphs are constructed. Transmission events are simulated at this resolution. Other disease state transitions are simulated at the end of each day. PanCitySim is a flexible framework that can be readily integrated with other activity-based mobility simulators. The pseudocode for the framework is provided in SI Note 6.

SEIRD model

We define the following states in our susceptible-exposed-infectious-recovered-deceased (SEIRD) model: susceptible (\mathbf{S}), exposed, i.e. infected but not contagious (\mathbf{E}), infectious and symptomatic (\mathbf{I}^S), infectious but asymptomatic (\mathbf{I}^A), recovered (\mathbf{R}) and deceased (\mathbf{D}). We assume that symptomatic cases are automatically quarantined by the end of the day.

The transitions to each of these states are governed by the following probabilities:

$$\phi_{n,t} = 1 - e^{(-\Theta \sum_m q_{m,t} \cdot i_{nm,t} \cdot \tau_{nm,t})} \quad (1)$$

$$\kappa_{n,d} = 1 - e^{-\frac{1}{d_L}} \quad (2)$$

$$\gamma_{n,d} = 1 - e^{-\frac{1}{d_I}} \quad (3)$$

$$\mu_{n,d} = 1 - e^{-\frac{1}{d_D}} \quad (4)$$

ϕ is the probability of infection, where Θ is a parameter to be calibrated. Using the mechanistic framework [4, 5], q is a measure of viral shedding rate [m^3] and i the contact intensity [$1/\text{m}^3$]. τ is the duration of contact. The indices are m (susceptible population), n (infectious) and t (time step). κ is the daily probability of transitioning from exposed \mathbf{E} to infectious $\mathbf{I}^{\{A,S\}}$ and d_L is the incubation period [8]. Furthermore, $d_L \sim \text{Lognormal}(\mu = 1.62, \sigma^2 = 0.42)$ [11]. The median incubation period is taken as 5 days [11]. ρ is the probability an infectious person is symptomatic. Thus, the transition to state \mathbf{I}^S is governed by the probability $\rho\kappa$. Further, α is the proportion of infectious people who are symptomatic, γ is the daily probability that a person recovers (d_I is the duration of infectiousness, also lognormally distributed) and μ is the mortality rate. Evidence suggests that ρ and μ are highly age-dependent [8]. Given that case fatality rates have been shown to differ significantly by age group, we use the values estimated by [10] to infer the number of days from symptom onset to death d_D , which is lognormally distributed with age-specific parameters. Details of the age-specific estimation of d_D (along with other SEIRD model explanations) are given in SI Note 1.

Contact intensity

The transmission probability is explicitly dependent on the separation distance and shedding rate [5]. With regard to distance, the contact intensity i has an inverse cube relationship. For simplicity, we assume the shedding rate (q_0) remains constant, but estimate the separating distance $d_{n,m}$ at time step t between two persons n and m at a given physical node V based on locations which are assumed to be normally distributed about the respective node center. We then calibrate for a fixed contact intensity i_0 , which we then scale by $\frac{1}{d_{n,m}^3}$ per node and time step. For agents in transit, we partition the vehicles into squares, randomly assign passengers to each square partition, and estimate the expected distance between randomly selected passenger pairs. When agents are at home, we use the expected distance between inhabitants based on the average square footage of homes in the city. Thus, the probability of transmission is given by:

$$\phi_{n,t} = 1 - \exp \left\{ -\Theta q_0 i_0 \sum_m \frac{1}{d_{n,m}^3} \cdot \tau_{nm,t} \right\} \quad (5)$$

Further details on the modeling and estimation of inter-person distances in transit vehicles and at activity locations are given in SI Note 2.

Contact network generation

A contact network is a collection of several contact graphs at different times of day. We generate contact graphs at 5 minute time steps for the entire population. For generation of graphs, we use the outputs from activity-based simulated trajectories from calibrated models of two cities. The contact graph, at any 5 minute time window, is created by a union of three sub graphs- home, activity

or transit. The *Home* graph consists of agents who share a home during the time window. The activity graph comprises individuals who are performing an activity (*Work*, *Education*, *Shopping* or *Other*). The *Transit* graph consists of individuals who are traveling in a bus or train or waiting for the same. We assume that motorists make no contacts while en route to their destinations, hence they are not modeled in our contact graph. To facilitate an efficient representation of the contact graphs, we employ a hub-and-spoke transformation, which leverages on the sparseness of the graphs. Details of the construction of the contact network are found in SI Note 3.

Calibration

To find Θ , we calibrate in order to achieve a basic reproductive number (average number of secondary cases caused by an infected person in the early stage of the epidemic) of $R_0 = 2.5$ using:

$$R_0 = \frac{1}{X} \sum_m^X \sum_n^S \left(1 - e^{-\Theta' \sum_m \tau_{nm}}\right) \quad (6)$$

where $\Theta' = \Theta q_0 i_0$, and X is the set of index cases while S the set of secondary cases [5]. We define R_0 as the average number of new infections per initially infected person. We calibrate R_0 over a period of 5 days on the full population, as this is the median duration of incubation [11]. Post calibration, R_0 was equal to 2.43 ± 0.14 in case of *Auto Sprawl* and 3.19 ± 0.16 in case of *Auto Innovative* using 30 samples for both cases (errors are 95% confidence intervals). The five-day average of R_t (daily reproductive rate), however was 0.77 in both cities. Further calibration considerations are noted in SI Note 4.

Validation

We partially validate the output from PanCitySim. The partial nature of the validation is due to two facts. First, the data available for the number of infections are only partially observed. This is attributed to the overstretching of health facilities, many cases going undetected and the cause of death not being attributed to COVID-19 due to several reasons. Second, as soon as the general population and the government are aware of the epidemic, several interventions are put in place to counter the spread. Since the testing of such mitigation measures as scenarios was out of the scope of this study, we do not fully match the reported case and mortality numbers.

We compare our prototype city simulation results with data reported from cities in the respective typologies: *Auto Sprawl* and *Auto Innovative*. Our findings are summarized in Figure 9. We also note that these contact networks are based on weekday activity models. However, since the framework is simulator agnostic, we can account for differences in weekend activity patterns by incorporating relevant travel models. Finally, to improve the prediction capabilities of this framework, weather patterns should be accounted for in order to reflect appropriate multimodal impacts on mobility and activity patterns.

Data availability

The full data set used for this study is publicly available. Given that the sizes of the data files used in our experiments are large, we have created a demonstration data set with 30000 individuals chosen randomly from *Auto Sprawl*, which can be downloaded from our Github repository for PanCitySim: <https://github.com/pancitysim/PanCitySim>. The links to the file-server hosting the full data set will also be maintained in the same location.

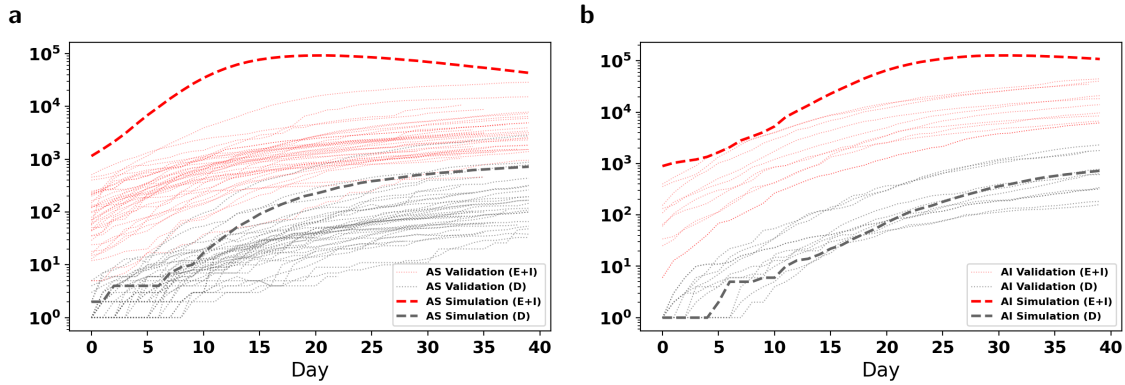


Figure 9. We compare simulation results to reported data on cases and mortalities. (a) *Auto Sprawl* (simulation) compared to other U.S. metropolitan areas in the same typology (e.g. Baltimore, Austin, Indianapolis). (b) *Auto Innovative* (simulation) compared to other U.S. metropolitan areas in the same typology (e.g. Boston, Chicago, San Francisco) Validation start dates were matched with earliest record of the first death. Data was obtained from the New York Times repository (<https://github.com/nytimes/covid-19-data>).

Code availability

An end-to-end working Python notebook with code and documentation of the epidemiological model is available for public download at <https://github.com/pancitysim/PanCitySim>. We discuss the computational performance of PanCitySim in SI Note 5, and provide pseudocode for the framework in SI Note 6.

References

- [1] A. R. Sahin, A. Erdogan, P. Mutlu Agaoglu, Y. Dineri, A. Y. Cakirci, M. E. Senel, R. A. Okyay, and A. M. Tasdogan, “2019 Novel Coronavirus (COVID-19) Outbreak: A Review of the Current Literature,” *EURASIAN JOURNAL OF MEDICINE AND ONCOLOGY*, vol. 4, no. 1, pp. 1–7, 2020.
- [2] W. J. McKibbin and R. Fernando, “The Global Macroeconomic Impacts of COVID-19: Seven Scenarios,” SSRN Scholarly Paper ID 3547729, Social Science Research Network, Rochester, NY, Mar. 2020.
- [3] J. Hackl and T. Dubernet, “Epidemic Spreading in Urban Areas Using Agent-Based Transportation Models,” *Future Internet*, vol. 11, p. 92, Apr. 2019.
- [4] S. A. Muller, M. Balmer, A. Neumann, and K. Nagel, “Mobility traces and spreading of COVID-19,” *medRxiv*, p. 2020.03.27.20045302, Mar. 2020.
- [5] T. Smieszek, “A mechanistic model of infection: Why duration and intensity of contacts should be included in models of disease spread,” *Theoretical Biology and Medical Modelling*, vol. 6, p. 25, Nov. 2009.
- [6] M. Adnan, F. C. Pereira, C. L. Azevedo, K. Basak, M. Lovric, S. Raveau, Y. Zhu, J. Ferreira, C. Zegras, and M. Ben-Akiva, “SimMobility: A Multi-scale Integrated Agent-Based Simulation Platform,” in *Transportation Research Board 95th Annual Meeting Transportation Research Board*, no. 16-2691, 2016/00/00.

- [7] T. Smieszek, M. Balmer, J. Hattendorf, K. W. Axhausen, J. Zinsstag, and R. W. Scholz, “Reconstructing the 2003/2004 H3N2 influenza epidemic in Switzerland with a spatially explicit, individual-based model,” *BMC infectious diseases*, vol. 11, p. 115, May 2011.
- [8] K. Prem, Y. Liu, T. W. Russell, A. J. Kucharski, R. M. Eggo, N. Davies, S. Flasche, S. Clifford, C. A. B. Pearson, J. D. Munday, S. Abbott, H. Gibbs, A. Rosello, B. J. Quilty, T. Jombart, F. Sun, C. Diamond, A. Gimma, K. van Zandvoort, S. Funk, C. I. Jarvis, W. J. Edmunds, N. I. Bosse, J. Hellewell, M. Jit, and P. Klepac, “The effect of control strategies to reduce social mixing on outcomes of the COVID-19 epidemic in Wuhan, China: A modelling study,” *The Lancet Public Health*, vol. 0, Mar. 2020.
- [9] J. B. Oke, Y. M. Aboutaleb, A. Akkinepally, C. L. Azevedo, Y. Han, P. C. Zegras, J. Ferreira, and M. E. Ben-Akiva, “A novel global urban typology framework for sustainable mobility futures,” *Environmental Research Letters*, vol. 14, p. 095006, Sept. 2019.
- [10] R. Verity, L. C. Okell, I. Dorigatti, P. Winskill, C. Whittaker, N. Imai, G. Cuomo-Dannenburg, H. Thompson, P. G. T. Walker, H. Fu, A. Dighe, J. T. Griffin, M. Baguelin, S. Bhatia, A. Boonyasiri, A. Cori, Z. Cucunubá, R. FitzJohn, K. Gaythorpe, W. Green, A. Hamlet, W. Hinsley, D. Laydon, G. Nedjati-Gilani, S. Riley, S. van Elsland, E. Volz, H. Wang, Y. Wang, X. Xi, C. A. Donnelly, A. C. Ghani, and N. M. Ferguson, “Estimates of the severity of coronavirus disease 2019: A model-based analysis,” *The Lancet Infectious Diseases*, vol. 0, Mar. 2020.
- [11] S. A. Lauer, K. H. Grantz, Q. Bi, F. K. Jones, Q. Zheng, H. R. Meredith, A. S. Azman, N. G. Reich, and J. Lessler, “The Incubation Period of Coronavirus Disease 2019 (COVID-19) From Publicly Reported Confirmed Cases: Estimation and Application,” *Annals of Internal Medicine*, Mar. 2020.
- [12] B.-h. Nahmias-Biran, J. B. Oke, N. Kumar, C. Lima Azevedo, and M. Ben-Akiva, “Evaluating the impacts of shared automated mobility on-demand services: An activity-based accessibility approach,” *Transportation*, Apr. 2020.
- [13] J. B. Oke, A. P. Akkinepally, S. Chen, Y. M. Aboutaleb, Y. Xie, C. L. Azevedo, C. Zegras, J. Ferreria, and M. Ben-Akiva, “Evaluating the systemic effects of automated mobility-on-demand services via large-scale agent-based simulation of auto-dependent prototype cities,” 2019.
- [14] J. Alstott, E. Bullmore, and D. Plenz, “Powerlaw: A Python Package for Analysis of Heavy-Tailed Distributions,” *PLOS ONE*, vol. 9, p. e85777, Jan. 2014.
- [15] A. D. Broido and A. Clauset, “Scale-free networks are rare,” *Nature Communications*, vol. 10, p. 1017, Mar. 2019.
- [16] A. J. Kucharski, T. W. Russell, C. Diamond, Y. Liu, J. Edmunds, S. Funk, R. M. Eggo, F. Sun, M. Jit, J. D. Munday, N. Davies, A. Gimma, K. van Zandvoort, H. Gibbs, J. Hellewell, C. I. Jarvis, S. Clifford, B. J. Quilty, N. I. Bosse, S. Abbott, P. Klepac, and S. Flasche, “Early dynamics of transmission and control of COVID-19: A mathematical modelling study,” *The Lancet Infectious Diseases*, vol. 0, Mar. 2020.
- [17] G. Lin, A. T. Strauss, M. Pinz, D. A. Martinez, K. K. Tseng, E. Schueller, O. Gatalo, Y. Yang, S. A. Levin, E. Y. Klein, and F. t. C. M.-H. Program, “Explaining the Bomb-Like Dynamics of

COVID-19 with Modeling and the Implications for Policy,” *medRxiv*, p. 2020.04.05.20054338, Apr. 2020.

- [18] D. Gunzler and A. R. Sehgal, “Time-Varying COVID-19 Reproduction Number in the United States,” *medRxiv*, p. 2020.04.10.20060863, Apr. 2020.

Acknowledgments

The authors acknowledge the support of the University of Massachusetts Amherst, Ariel University and Singapore-ETH Centre in providing resources for carrying out this work. The authors would also like to acknowledge the support of Prof. Martin Raubal, ETH Zurich.

Author contributions

B. N-B., J.O. and N. K. designed the study and implemented the method. N. K. implemented the simulations. J.O. and B. N-B. supported with data acquisition. B. N-B., J.O. and N. K. analyzed the results and wrote the manuscript.

Competing interests

The authors declare no competing interests.